

# ROTOR LOADS PREDICTION USING ESTIMATED MODAL PARTICIPATION FROM SENSORS

<b>Gang Wang</b>	<b>A. Abhishek</b>	<b>Inderjit Chopra</b>	<b>Nam Phan</b>	<b>Daniel Liebschutz</b>
Principal Engineer	Research Asst.	Alfred Gessow Professor	Branch Head	Engineer
Techno-Sciences Inc.	Alfred Gessow Rotorcraft Center		Structural Division - Air 4.3.3.2	
11750 Beltsville Dr.	University of Maryland		Naval Air Systems Command	
Beltsville, MD 20705	College Park, MD 20742		Patuxent River, MD, 20670	

## ABSTRACT

The accurate prediction of loads/stresses in rotor and dynamic components is a key step towards the goal of an efficient Structural Health and Usage Monitoring (SHUM) for rotorcraft. This paper discusses the prediction of vibratory loads in a typical articulated rotor using combined analytical and experimental approach. The airloads are derived based on a few blade strain sensor measurements in conjunction with the refined lifting-line aerodynamic model. The modal components of the deformation geometry is estimated using measurements from sensors located in the rotating frame. Based on the updated blade deflection inputs, the airloads are calculated, which are then used for the prediction of rotor load/stress. Systematic loads prediction validation is conducted using the newly-developed airloads derivation approach for the Black Hawk (UH-60A) in steady level and unsteady maneuver flight conditions. Better correlation with flight test data is observed for airloads and structural loads when compared with the baseline lifting-line predictions without any sensor data. The lifting-line aerodynamic model needs to be further improved to enable the prediction of maneuver loads accurately, especially for the blade pitching moment.

## INTRODUCTION

Helicopter rotors and their associated dynamic components operate in high-cycle challenging environments. Major factors that impact the rotor system maintenance are: fatigue in the rotor hub dynamic components (spherical bearings, bushings, push-rods, root end couplings, etc), operational impact-damage due to ballistic and Foreign Object Damage (FOD) in the rotor blade, and out-of-track rotor condition. It is important to develop and refine technologies that manage and mitigate the sources of vibratory loads through prognostics. Maley et. al. [1] provided an overview of the Navy's Structural Health and Usage Monitoring (SHUM) practices for their rotary wing aircraft. Currently, the Navy is trying to implement SHUM features in the V-22, CH-53E, MH-60R/S, and H-1Y/Z. In order to achieve the goal of a successful

SHUM system in a rotorcraft, the accurate prediction of loads/stresses in rotor and dynamic components is an important step. Datta et. al. [2] presented an overview on rotor loads prediction using a coupled Computational Fluid Dynamics (CFD) and Computational Structural Dynamics (CSD) methodology. The focus was on steady level flight, where most of the CFD/CSD analyses have been attempted. The application of CFD in rotorcraft problems has evolved over the past twenty years as a viable means to improve the aerodynamic modeling in rotorcraft comprehensive analyses. The complexity of the solution procedure for an unsteady maneuver has been the primary barrier towards a first principle based prediction of loads. The availability of detailed flight test data including blade pressures for the Utility Tactical Transport Aircraft System (UTTAS) pull-up maneuver provided an impetus for the validation of high fidelity simulation as carried out by Bhagwat et. al. (Refs. [3, 4]), using a multibody finite element structural model coupled with a Reynolds Averaged Navier-Stokes (RANS) model. This work demonstrated RANS capability in predicting two ro-

---

Presented at the 39<sup>th</sup> European Rotorcraft Forum, Paris, France, September 9–11, 2010.

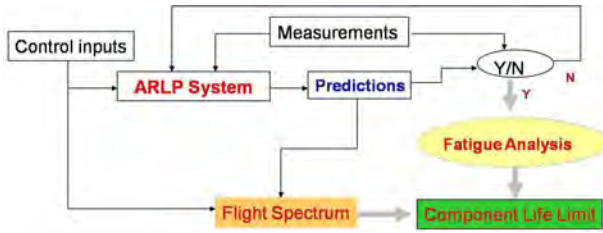


Figure 1: Schematic of ARLP system in SHUM

tor dynamic stall cycles for a maneuver. Even though the analysis was not able to resolve the mechanism of advancing blade stall observed during the pull-up maneuver, it showed that the oscillatory blade structural loads could be predicted with increased accuracy using isolated rotor calculations. Only recently the mechanism of advancing blade stall in an unsteady pull-up maneuver has been resolved and understood through the separation of the physics of structural dynamics and aerodynamics (Ref. [5]).

However, even if analytical predictions are accurate, the actual flight conditions and resulting loading spectrum are not known with sufficient accuracy to predict stresses in rotor dynamic components. At this time, the state-of-art in the prediction of rotor loads is not robust for maneuvering and many other flight conditions. Not only further refinements in comprehensive analysis tools is needed, but also detailed load measurements under controlled environment are needed for systematic validation of the rotor analysis. By leveraging the rotor and dynamic components measurement data from flight tests, we developed a combined analytical and experimental approach to significantly improve the accuracy of predictions of loads and stresses in dynamic components. These predictions are carried out without detailed actual flight condition data and loading spectrum.

## ARLP SYSTEM

In this study, an Advanced Rotorcraft Load Prediction (ARLP) system is developed, which features the combined analytical and experimental methodology to carry out load prediction of rotor and dynamic components. This ARLP system exploits the University of Maryland Advanced Rotorcraft Code (UMARC) [6, 7] with updated features such as the refined lifting-line aerodynamics, time-marching free wake model, multibody rotor dynamic modeling, and swashplate dynamics. A closed-loop ARLP system was developed as shown in Fig. 1. The airloads are derived based on a few blade strain sensor measurements in conjunction with the lifting-line comprehensive analysis. Based on these updated airload inputs, the load/stress prediction of rotor and dynamic components is refined. Systematic load correlations were

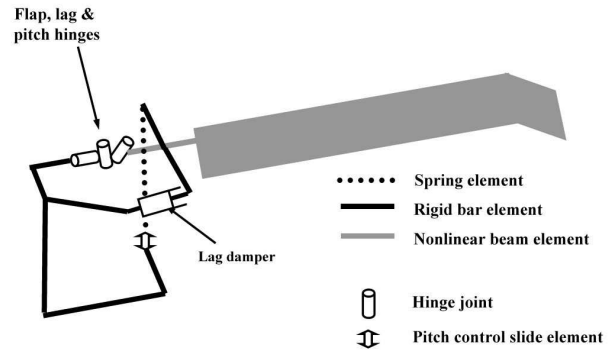


Figure 2: Schematic of the UH-60A structural model used in UMARC2

carried out for several different flight conditions using the newly-derived analysis. The Black Hawk UH-60A flight test data [8] were used to validate our prediction results.

## Multibody Rotor Dynamic Model

The structural dynamics model used is an enhanced version of the UMARC (Ref. [6, 7]). The rotor model (see Fig. 2) consists of flexible blades, rigid root end control components, and a swashplate model. Each blade is modeled as a fully articulated beam with coincident flap and lag hinges at 4.66% span. It is discretized using 20 nonlinear beam elements, and each nonlinear beam elements has a local frame of reference attached to it in order to model arbitrary large deformations. The swept portion of the blade is modeled using 3 elements with swept elastic axis. The pitch horn and the hub is modeled using rigid body elements, and the pitch link is modeled as a linear spring-damper element. The pitch-link stiffness is obtained from the measured equivalent root torsion spring stiffness of 1090 ft-lbs/deg [9], reduced using the undeformed pitch-horn length. The blade dynamics equations are updated to include the gyroscopic contributions to the rotor resulting from the vehicle linear and angular accelerations.

## Swashplate Model

The swashplate is modeled as a thin disk with 3 degrees of freedom: vertical heave, pitch-up, and roll-left. It is attached to the four pitch links on the top, and three servo actuators at the bottom (Fig. 3). The rotating and the non-rotating swashplates are idealized together as a single functional element which: (1) transfer loads between the servos at the bottom and the pitch links on the top, (2) transfer displacements from servos at the bottom to the pitch links at the top. The pitch links, and the servos are modeled as linear spring-damper systems. The details of the structural model, and determination of swash-

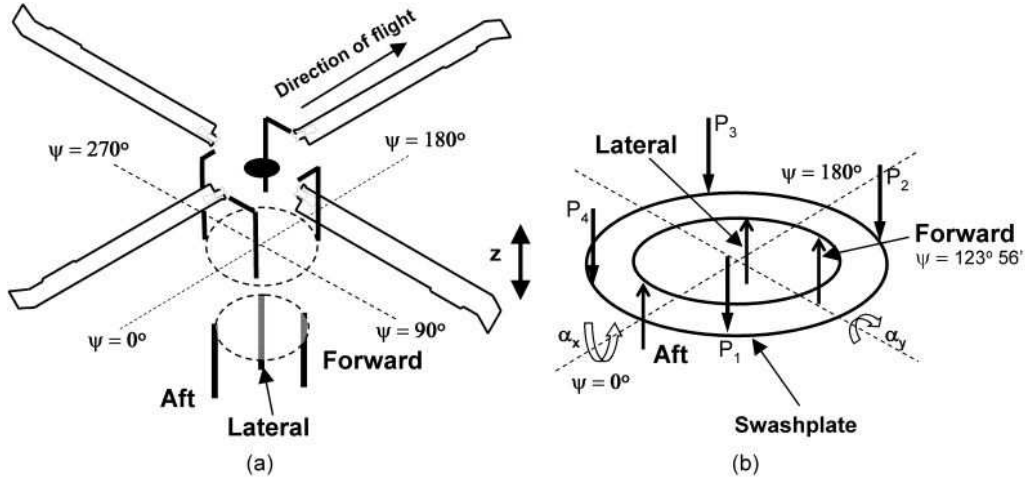


Figure 3: Schematic of UH-60A Blade-Swashplate model; (b) Detailed Swashplate model with 3 servo actuators (forward, aft and lateral) and four pitch-links (P1, P2, P3 and P4)

plate and servo properties is available in Ref. [7].

### *Lifting-Line Aerodynamic Model*

A multi-bladed transient lifting-line aerodynamic model is included, which incorporates 2-D airfoil property tables, a Weissinger-L near wake model, a time domain representation of free wake model, and the Leishman-Beddoes dynamic stall model [11] for attached and separated flows.

At each azimuth (i.e. time), the inputs into the aerodynamic model are the blade deformations for all blades, the instantaneous advance ratio, shaft tilt angle, the rotor pitch and roll angles and angular rates, and the control angles. The outputs from the model are the airloads on all blades, and the inflow velocities at the blade control points (swept 3/4 chord line). Within the model, the current blade deformations are used along with the inflow velocities, stored from the previous time step, to calculate the airloads, bound circulation distribution, near wake trailer strengths, and near wake induced velocities at the blade control points. The near wake induced velocities are then used to re-calculate the airloads. The bound circulation distribution and the current blade deformations are then used to advance the free wake solution to the current time step. This free wake solution is used in the calculation of airloads in the next time step. The free wake model of Ananthan-Leishman [12] is modified to incorporate flexible blade deformations in flap, lag, and torsion, and the bound circulation strengths as calculated above. For the analysis at high speed flight conditions, two wake turns are used for the analysis, and a wake discretization angle of  $5^\circ$  is used.

The wake models account only for trailed vorticity, the effect of shed vorticity is incorporated using the Leishman-Beddoes unsteady aerodynamic model. At each time step, the unsteady model is updated

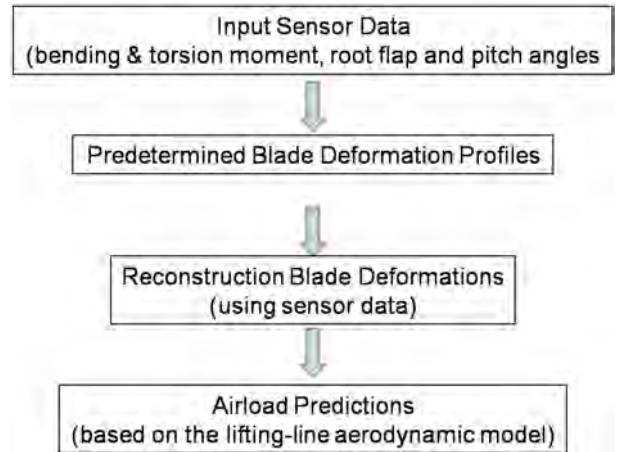


Figure 4: Airloads determination scheme using sensor measurements

based on the change in airloads from the previous time step. The unsteady model is based on the effective section angles of attack after including free wake and near wake effects. The transient aerodynamic analysis was validated in Ref. [14] for level flight conditions.

## DEVELOPMENT OF AIRLOADS DERIVATION MODEL

Airloads are derived using a few measured blade sensor data. This approach, called the Direct Airload Derivation Model, is described in Fig. 4. In this approach, first the blade rotating coupled mode shapes are obtained using eigen analysis of the mass and stiffness matrix of the blade obtained from finite element

analysis. Next, the deformed blade geometry is represented by a linear combination of the mode shapes. The flight test sensor data measured in the rotating frame (root angles, bending moments etc.), is then used to determine the *modal* contributions. For the present analysis four flap modes, two lag modes and two torsion modes are used, thereby necessitating the use of at least 8 sensor data. Use of more sensors typically improves the accuracy of deformation geometry estimation.

The blade nodal degrees of freedom can be described using the following expression

$$\{q\} = \sum_{i=1}^N \Phi_i(r) \xi_i(t) \quad (1)$$

where,  $N$  is the total number of modes used,  $\Phi_i$  is the coupled eigen vector associated with mode  $i$  and  $\xi_i$  is the corresponding *modal* coordinate. The eigen vector matrix for the blade structural model is evaluated using Finite Element Analysis. The goal is to determine the modal coordinates, which appears straight forward if the left hand side of the above equation is precisely known. But in reality only few elements of the nodal degrees of freedom vector are known, either via direct measurements or derived from the available sensor data. This partial information is used to set-up a set of linear equations which can be solved for  $\xi_i$  at every time step. Therefore, at least  $N$  equations has to be set-up. The time history of blade flap, lag and torsion deformation at root is available from the flight test, and this constitutes three equations. The bending and torsion moments data at various locations are also available. The blade flap bending moment at any point along the blade span, can be expressed in terms of the blade nodal degrees of freedom, which can then be equated to the right hand side of the equation to obtain additional linear equations. Accuracy of the solution increases with the number of sensor data used. This is because the resulting system of equation is of the form  $AX = B$ , where  $A$  is not a symmetric matrix. The system of equation with the number of rows of  $A$  greater than the number of columns is known as an overdetermined system. The solution  $X$  in this case is the least squares solution, that minimizes the norm of vector  $(A * X - B)$ .

Once the modal coordinates are estimated, it can be substituted in the above equation to obtain the complete nodal degree of freedom vector which in turn determines the radial variation of blade deformations. This process is repeated at each time step to obtain the deformation time history of the blade. The sensor data used for the implementation of the present airload derivation model are: (1) root pitch, flap and lag angles; (2) flap bending moment at 30%, 50%, 70% and 90% R stations; (3) torsion moment at 30% and 70% R and (4) lag moment at 30% R. It should be

noted that the data set needed for the airloads derivation model does not need be the same as listed above, and the loads derivation model can be easily adapted to make use of available sensor data by reducing the number of modes used of the deformation estimation.

Once the deformations has been estimated, the airloads can then be calculated directly using the lifting-line aerodynamic model, which can then be applied to the structural model in an uncoupled manner for the prediction of structural loads.

## RESULTS

### *Steady State Flight (C8534)*

Flight test data from the UH-60A high speed level flight 8534 ( $C_W/\sigma = 0.0783$ ,  $\mu = 0.368$ ) is used to validate the predictions using airload derivation model. The high speed flight is a high vibration flight, and is characterized by the transonic shock effect observed in the blade pitching moment on the advancing side.

The normal force predictions obtained using derived blade deformations show significant improvement over the baseline predictions obtained using trim controls (without any sensor data based corrections), as shown in Fig. 5. The key improvement lies in the phase of the negative lift peak observed between  $90^\circ$ – $180^\circ$ . The conventional lifting-line model is unable to predict this phase angle accurately due to less accurate pitching moment and resulting elastic twist. The airloads derivation model uses sensor data to improve blade elastic twist angle calculations, thereby resulting in accurate phase angle prediction. Further, the peak-to-peak magnitude of the predicted normal force also shows significant improvement, especially in the outboard regions, e.g. the normal force at 99%R using the baseline analysis is under-predicted by 30%, while that obtained using derived blade deformations is over-predicted by only 10%.

The pitching moment predictions do not show the same level of improvement in general due to inherent limitation of the lifting-line model in prediction of blade pitching moment, as shown in Fig. 6. It should be noted that the lifting-line analysis as such has its own limitations and is unable to capture the advancing blade transonic stall observed in the flight test pitching moment data.

The airloads obtained above is then used to calculate the structural loads. The derived airloads are imposed on the multi-body structural model, where an additional artificial damping is introduced in the simulation to mimic aerodynamic damping characteristics. Typically, 0.02% of critical structural damping is used and retained throughout the analysis, requiring 50 revolutions for the attainment of the steady state. The flap bending moment at 50% R and tor-

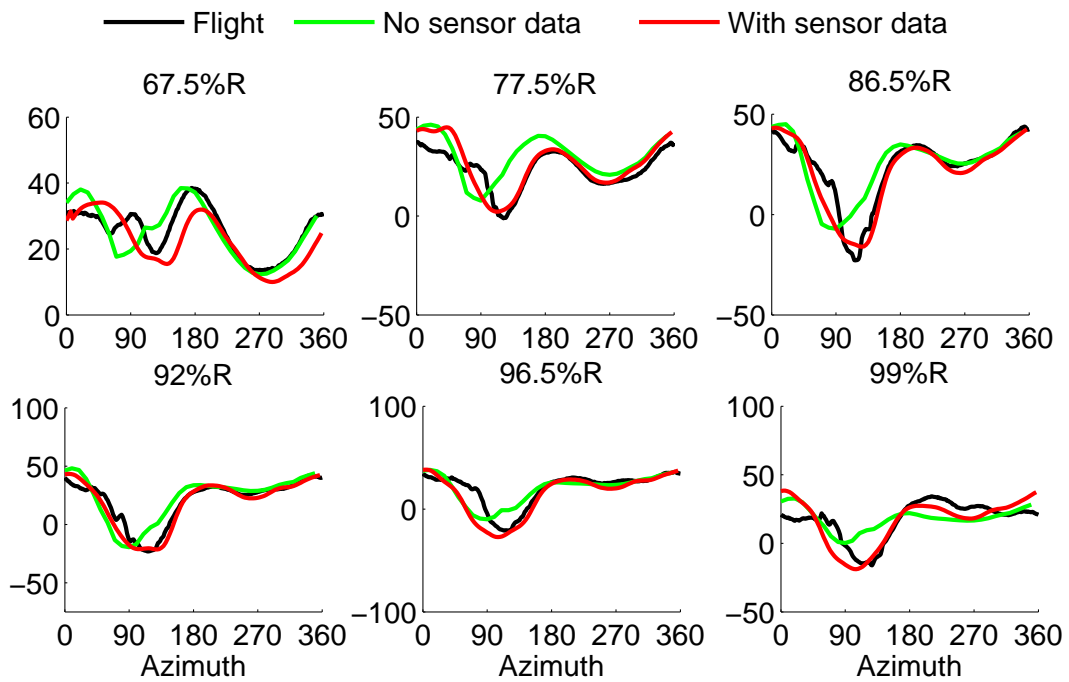


Figure 5: Comparison of normal force predicted during high speed steady flight C8534 using sensor data; ( $C_W/\sigma = 0.0783$ ,  $\mu = 0.368$ )

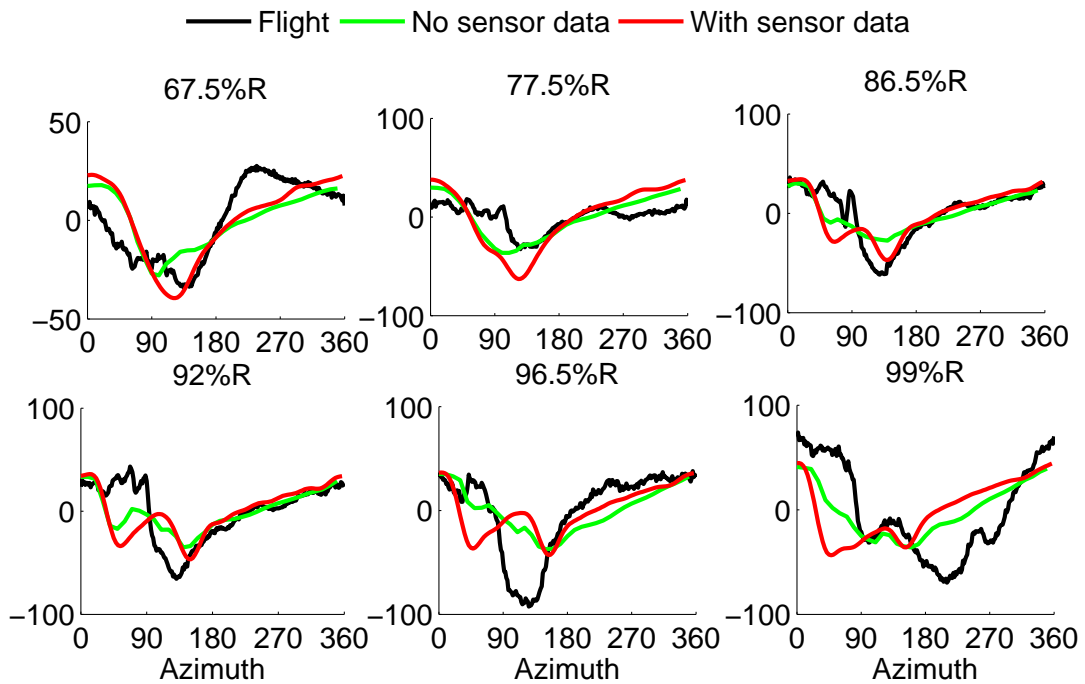


Figure 6: Comparison of pitching moment predicted during high speed steady flight C8534 using sensor data; ( $C_W/\sigma = 0.0783$ ,  $\mu = 0.368$ )

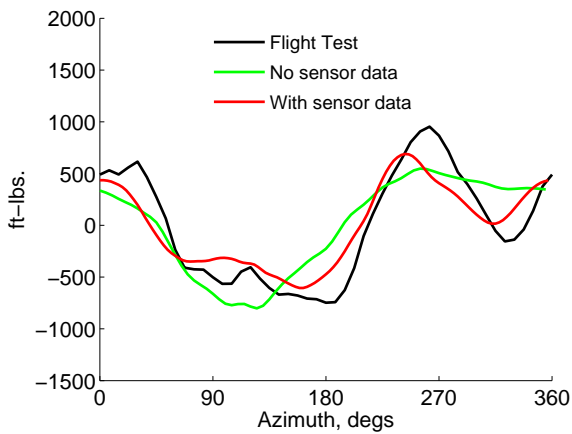


Figure 7: Comparison of predicted flap bending moment at 50%R during high speed steady flight C8534 using airloads derived from sensor data; ( $C_W/\sigma = 0.0783$ ,  $\mu = 0.368$ )

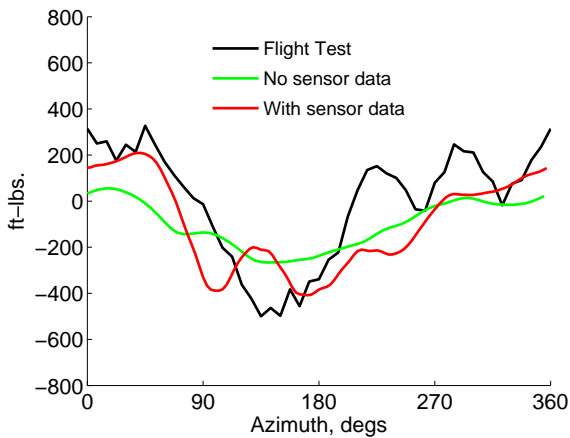


Figure 8: Comparison of predicted torsion moment at 30%R during high speed steady flight C8534 using airload derived from sensor data; ( $C_W/\sigma = 0.0783$ ,  $\mu = 0.368$ )

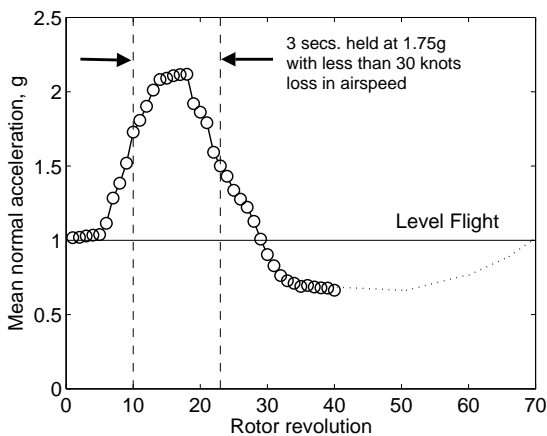


Figure 9: Mean load-factor for C11029 pull-up maneuver measured during the flight test

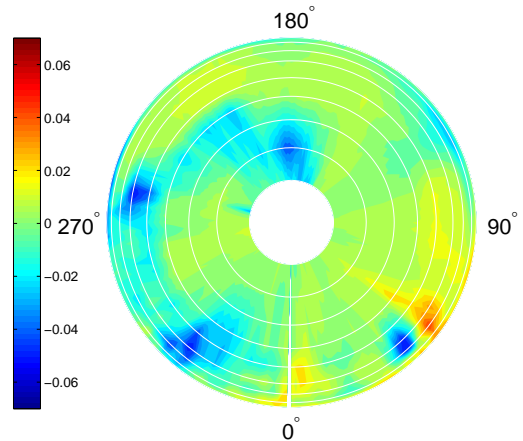


Figure 10: Contour map of non-dimensional flight test Pitching Moment C11029

sion moment at 30% R are shown in Figs. 7 and 8 respectively. It is observed that predicted structural loads show improvement in peak-to-peak magnitude when compared to the baseline lifting-line case without any sensor data based corrections. Due to the inherent deficiency of pitching moment prediction using the lifting-line aerodynamic model, torsion moment predictions are less satisfactory.

### Maneuver Flight (C11029)

Flight 11029 is a dynamic Utility Tactical Transport Aircraft System (UTTAS) pull-up maneuver that reaches 2.12g at 139 knots and produces the highest root flap bending moment with the third highest oscillatory pitch link load of all the UH-60A maneuvers. The peak to peak pitch link loads at this flight are 20% higher than those encountered during free engagement Air-to-Air Combat Test (AACT) flights of similar kind [17].

The entire maneuver is composed of 40 revolutions, with the first 5 – 6 revolutions corresponding to steady level flight regime similar to high-speed flight case. Revolutions 6 – 11 represent the transient conditions leading to the high load-factor period during 11 – 20 revolutions reaching up to 2.12g, after which the vehicle again transitions towards steady level flight condition as shown in Fig 9. Figure 10 shows the flight test pitching moment for the revolution 14 of UTTAS pull-up maneuver during the high load factor regime. The contour map shows sharp gradients representing three distinct stall cycles as noted by Ref. [18]. The first stall represented by the gradient on the retreating side near 270° azimuth is the stall due to high angle of attack resulting from high control angle settings. The second stall observed 70° or 1/5<sup>th</sup> revolution later occurs due to the re-attachment and then re-separation of the flow

triggered by the elastic twist. The third stall observed on the advancing side is a shock triggered flow separation [5]. Prediction of all three stalls is a challenge and even the most sophisticated coupled CFD/CSD analysis can only predict the two stalls on the retreating side [19].

Figure 11 shows the predicted normal force, obtained using derived deformations from the sensor data, for the pull-up maneuver at 86.5% $R$ . It can be observed that the predictions using sensor data show better correlation with flight test data for all revolutions, when compared with the baseline coupled lifting-line model. The pitching moment prediction is shown in Fig. 12 from which it is concluded that the airload derivation model developed in this paper is able to predict all three stall cycles. The prediction of all three stall cycles is possible because of accurate 5/rev elastic twist (see – Fig. 13) in the blade deformations derived from sensor data, which is missing in the deformation obtained using coupled lifting-line analysis. It should be noted that 5/rev elastic twist is critical in prediction of all three stalls [5].

The predicted flap bending moment at 50% $R$  and torsion moment at 30% $R$  for the C11029 maneuver are shown in Figures 14 and 15, respectively. The predictions using the sensor data show better correlation in phase and peak-to-peak magnitude. The flap bending moment prediction has correct phase because the predicted lift with sensor data has proper phase due to accurate elastic twist calculated from the blade sensor data. The torsion moment shows better peak-to-peak correlation with the test data during the steady flight regime. During the high load factor regime of the maneuver, the torsion moment prediction does show better higher harmonic content, but in general the peak-to-peak magnitude is under-predicted.

While the improvements observed in the airloads prediction using the sensor data is reflected in the predicted structural loads, which means that the accurate airloads lead to accurate structural loads prediction. The airloads were derived using only a few bending moment measurements. Further improvements is expected with the inclusion of more sensor monitoring measurements and flight parameters.

## CONCLUSIONS

In this paper, an airloads derivation methodology was developed using measurements from sensors in the rotating frame and the airload and structural load predictions for rotor dynamic components is validated using the UH-60 flight test data under both steady flight condition (C8534) and an unsteady maneuver (C11029). The airloads derivation methodology developed provides a simplified approach for calculation of blade loads. The structural loads (bending

moment, pitch-link load etc.) are easier to measure and can be used for accurate derivation of airloads, thereby facilitating an alternative to actual pressure measurements for calculation of airloads, especially during flight tests. To estimate modal participation, test data from ten sensors was used. Based on this study the following conclusions can be drawn:

1. Accurate blade deformations can be derived from the sensor measurements in the rotating frame, allowing for improved prediction of airloads and blade loads using a lifting-line based analysis.
2. The normal force predicted using the calculated deformations from the blade sensor data shows correct negative lift phase for both steady level high speed flight as well as the unsteady pull-up maneuver, thereby validating the derived blade elastic twist deformation. The peak-to-peak magnitude of normal force shows improved correlation with the flight test for the outboard stations, e.g. the normal force at 99% $R$  using the baseline lifting-line analysis is under-predicted by 30%, while that obtained using derived blade deformations is over-predicted by only 10%.
3. The blade pitching moment obtained using the estimated deformations from sensors predict all three stall cycles for the UTTAS pull-up maneuver due to accurate 5/rev elastic twist component. The magnitude of the stall peaks is significantly under-predicted due to inherent limitations of lifting-line analysis.
4. The structural loads predicted using the calculated airloads from the derived blade deformations show improvement in peak-to-peak magnitude when compared to the baseline lifting-line analysis.

In future work, the incorporation of more sensor data (such as pitch-link load, hub loads etc.) in the airloads derivation scheme would be investigated for refining the current model.

## ACKNOWLEDGMENT

Research support under the NAVAIR Phase II SBIR contract No. N68335-09-C-0186 (H-53 Heavy Lift Program Office: Dr. Michael Yu) is gratefully acknowledged.

## REFERENCES

- [1] Maley, S., Plets, J., Phan, N.D., "US Navy Roadmap to Structural Health and Usage Monitoring - The Present and Future," Presented at the American Helicopter Society 63<sup>rd</sup> Annual Forum, Virginia Beach, VA, May 1-3, 2007

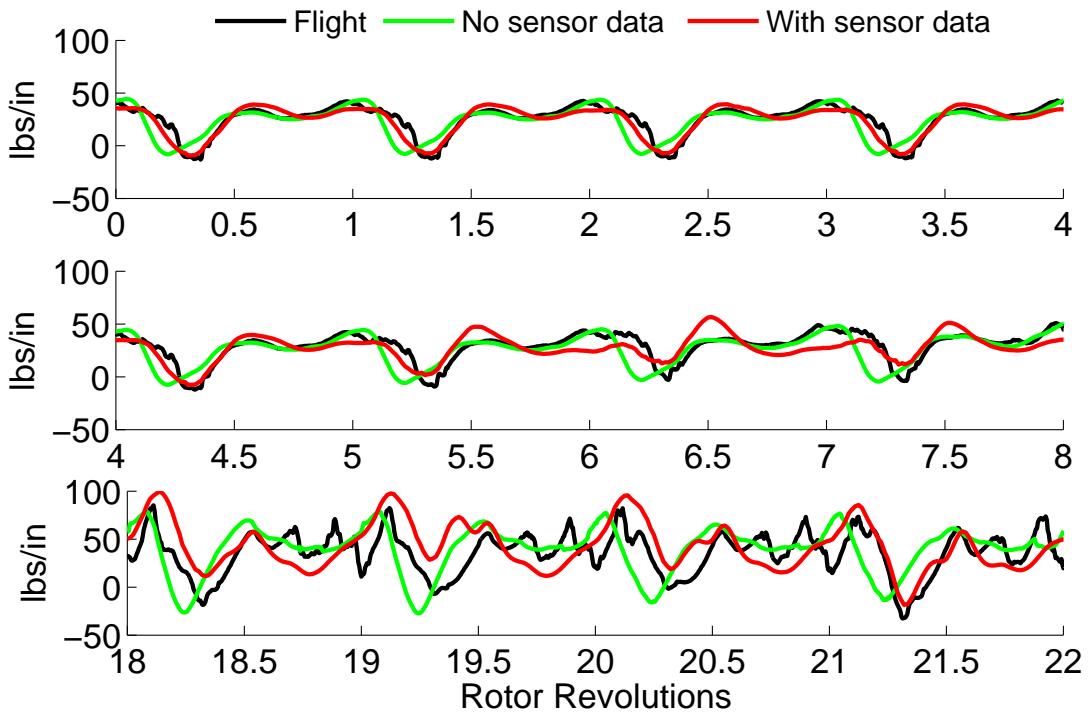


Figure 11: Predicted normal force for UTTAS pull-up maneuver C11029 using sensor data at 86.5%R

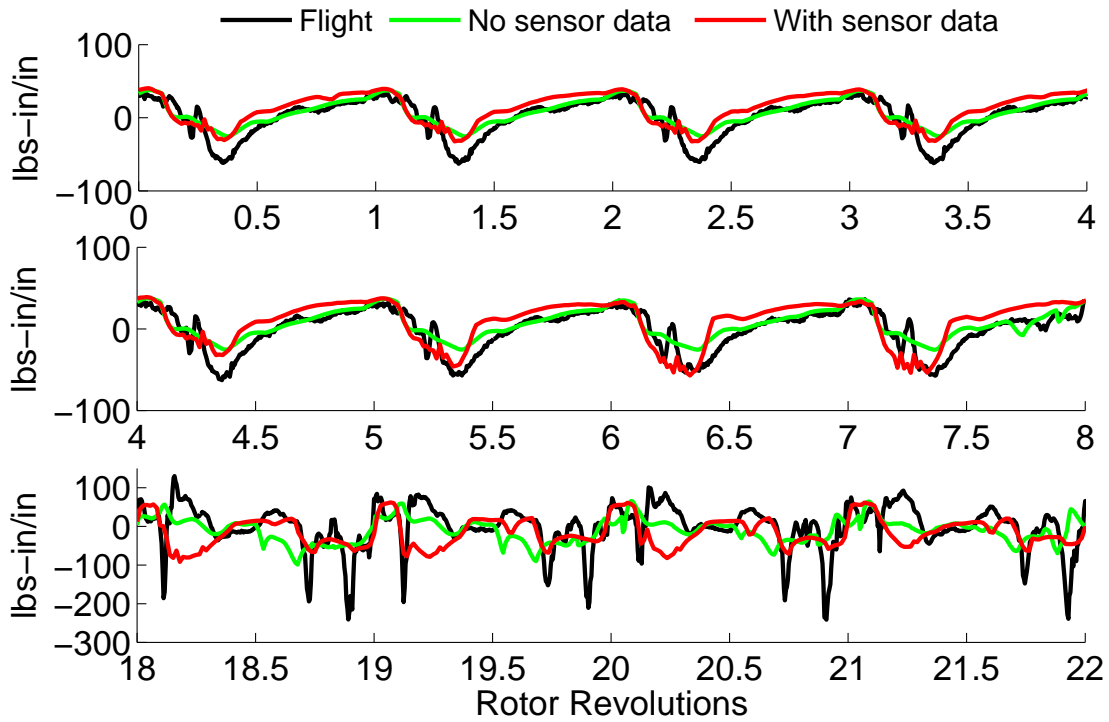


Figure 12: Predicted pitching moment for UTTAS pull-up maneuver C11029 using sensor data at 86.5%R

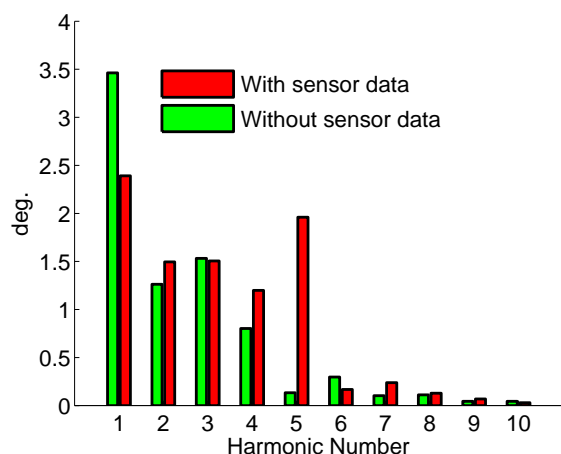


Figure 13: Comparison of blade elastic twist harmonic at tip for revolution 18 of UTTAS pull-up maneuver C11029

- [2] Datta, A., Nixon, M., Chopra, I., “Rotor Loads Prediction with the Emergence of Rotorcraft CFD,” *Journal of the American Helicopter Society*, 52 (4), pp – 287–317 Oct 2007.
- [3] Bhagwat, M. J., Ormiston, R. A., Saberi, H. A., and Xin, H., “Application of CFD/CSD Coupling for Analysis of Rotorcraft Airloads and Blade Loads in Maneuvering Flight,” American Helicopter Society 63<sup>rd</sup> Annual Forum Proceedings, Virginia Beach, VA, May 1-3, May 2007.
- [4] Bhagwat, M. J. and Ormiston, R. A., “Examination of Rotor Aerodynamics in Steady and Maneuvering Flight using CFD and Conventional Methods,” American Helicopter Society Specialists’ Conference on Aeromechanics, San Francisco, CA, January 2008.
- [5] Abhishek, A., Ananthan, S., Baeder, J., and Chopra, I., “Prediction and Fundamental Understanding of Stall Loads in UH-60A Pull-up Maneuver,” Presented at 66<sup>th</sup> Annual Forum of the American Helicopter Society, Phoenix, AZ, May 11–17 2010.
- [6] Bir, G., Chopra, I., Nguyen, K., “Development of UMARC (University of Maryland Advanced Rotor Code),” Proceedings of the 46th Annual National Forum of the American Helicopter Society, Washington, D.C, May 1990, pp. 55-70.
- [7] Abhishek, A., Datta, A., and Chopra, I., “Prediction of UH-60A Structural Loads Using Multi-body Analysis and Swashplate Dynamics,” *Journal of Aircraft*, Vol. 46, No. 2, March 2009.
- [8] Kufeld, R. M., Balough, D. L., Cross, J. L., Studebaker, K. F., Jennison, C. D., and Bousman, W. G., “Flight Testing of the UH-60A Airloads Aircraft,” American Helicopter Society 50th Annual Forum Proceedings, Washington, D. C., May 1994.
- [9] Kufeld, R. M., “High Load Conditions Measured on a UH-60A in Maneuvering Flight,” *Journal of the American Helicopter Society*, Vol. 43, (3), July 1998, pp. 202–211.
- [10] Weissinger, J., “The Lift Distribution of Swept-Back Wings,” National Advisory Committee for Aeronautics, Technical Memorandum No. 1120, 1942.
- [11] Leishman, J. G., and Beddoes, T. S., “A Semi-Empirical Model for Dynamic Stall,” *Journal of the American Helicopter Society*, Vol. 34, No. 3, July 1989, pp. 3–17.
- [12] Ananthan, S., and Leishman, J. G., “Helicopter Wake Dynamics During Tactical Maneuvers,” Proceedings of the 60<sup>th</sup> Annual Forum of the American Helicopter Society International, Baltimore, MD, June 7 – 10 2004.
- [13] Johnson, W., “Wake Model for Helicopter Rotors in High Speed Flight,” NASA CR 177507, Nov. 1988.
- [14] Abhishek, A., Datta, A., and Chopra, I., “Comprehensive Analysis, Prediction, and Validation of UH-60A Blade Loads in Unsteady Maneuvering Flight,” American Helicopter Society 63<sup>rd</sup> Annual Forum Proceedings, Virginia Beach, VA, May 1–3, 2007.
- [15] Hooper, W. E., “Vibratory Airloading of Helicopter Rotors,” *Vertica*, Vol. 8, No. 2, 1984, pp. 7392.
- [16] Datta, A., “Fundamental Understanding, Prediction and Validation of Rotor Vibratory Loads in Steady-Level Flight,” Ph.D. Dissertation, Dept. of Aerospace Engineering, University of Maryland, College Park, MD, 2004.
- [17] Washuta, K. W. and Stocker, B. P., Air-to-Air Combat Test (AACT II) Maneuvering Flight Loads for UH-60A and AUH-76 Helicopters, US-AAVSCOM TR-86-D-1, April 1986.
- [18] Kufeld, R. M. and Bousman, W. G., “UH-60A Helicopter Rotor Airloads Measured in Flight,” *The Aeronautical Journal of the Royal Aeronautical Society*, May 1997
- [19] Abhishek, A., Silbaugh, B., Ananthan, S., Baeder, J., and Chopra, I., “Coupled CFD/CSD Analysis of A Prescribed Pull-up Maneuver”, 3<sup>rd</sup> International Basic Research Conference on Rotorcraft Technology, Nanjing, China, Oct. 1416, 2009.

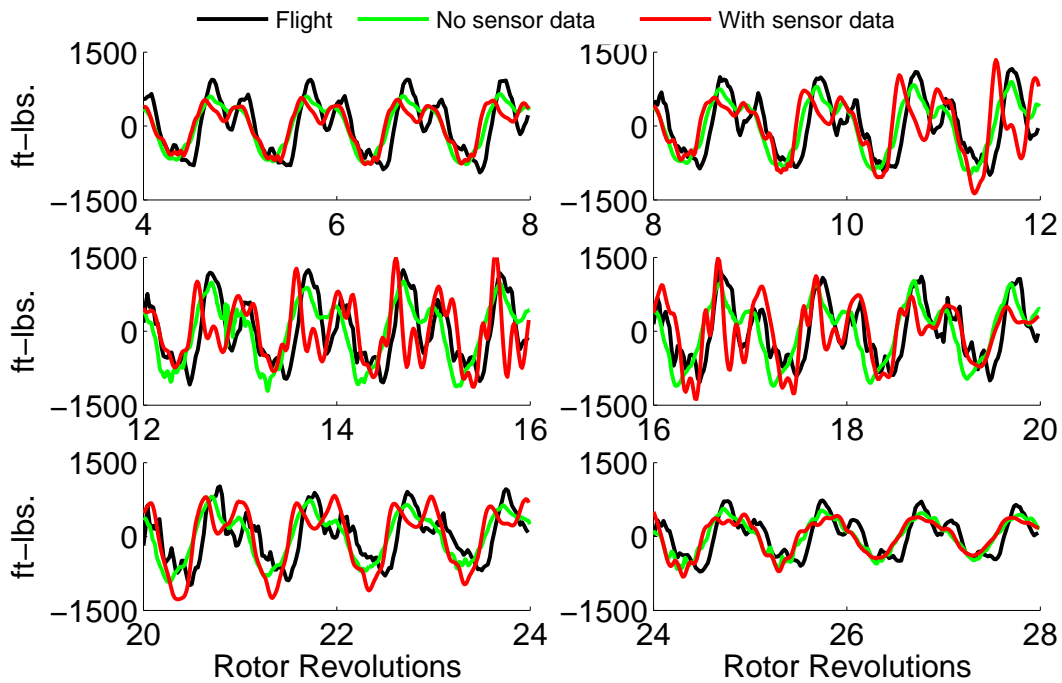


Figure 14: Predicted flap bending moment for UTAS pull-up maneuver C11029 using sensor data at 50% $R$ ; mean removed

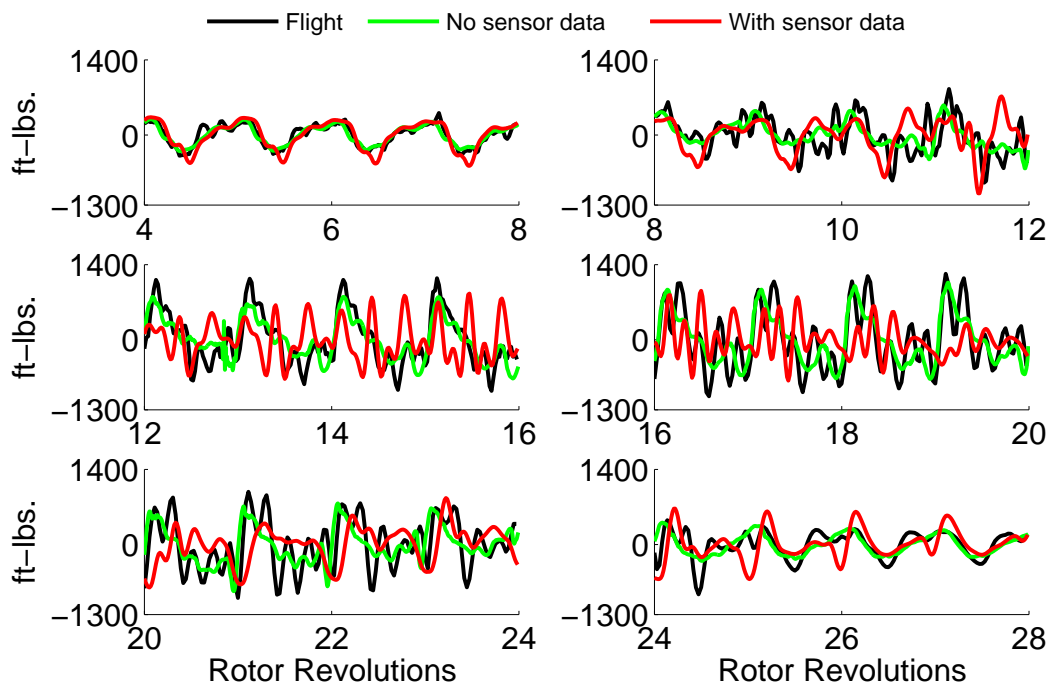


Figure 15: Predicted torsion moment for UTAS pull-up maneuver C11029 using sensor data at 30% $R$ ; mean removed